

Critical phenomena in atmospheric precipitation—Supplementary Information

Ole Peters and J. David Neelin

Contents

Supplementary Figures and Legends

See sections in which supplementary figures are referenced.

I. Supplementary Methods

- A. Rescaling factors in Fig. 1 1
- B. Order parameter pick-up in liquid water 2

II. Supplementary Discussion

- A. Sea surface temperature dependence 2
- B. Synoptic examples 3

III. Supplementary Equations

- A. Nontrivial variance-decrease implies scale-free correlation decay 4

Supplementary Notes (References) 5

I. SUPPLEMENTARY METHODS

A. Rescaling factors in Fig. 1

In Fig. 1 of the main text we show the order parameter pick-up and an associated increase in variance near the critical point. In comparing different regions we rescale the variables. Here we show the steps in this process for all four regions. The column-integrated water vapour w is multiplied by a factor f_w^i that reflects the different values of w_c in the climatic regions i . We could alternately have normalised by w_c , but the dimensional values are also of interest, so we retain the dimensional scale for the Western Pacific. We also multiply the mean precipitation $\langle P \rangle(w)$, with factors f_P^i , which reflect differences in capacity of the regional mechanisms to produce intense rainfall. These factors are here determined empirically from the fit of Eq. (1) of the main text above w_c .

The effect of the rescaling is shown in Fig. S1 through Fig. S3 for all four tropical oceanic regions we consider. In Fig. S1, the original curves exhibit substantial differences, although with hints of the underlying similarity of form. The values of w_c for Western Pacific, Eastern Pacific, Indian and Atlantic regions respectively, are 66.2, 63.7, 66.8, and 61.8 mm. Rescaling w by the ratio of the Western Pacific value over the regional value yields Fig. S2. This causes the locations of the steep pick-ups on the w -axis to coincide for all regions, but leaves the amplitudes for the Eastern Pacific and Atlantic at clearly lower values than for the other two regions. With rescaling of

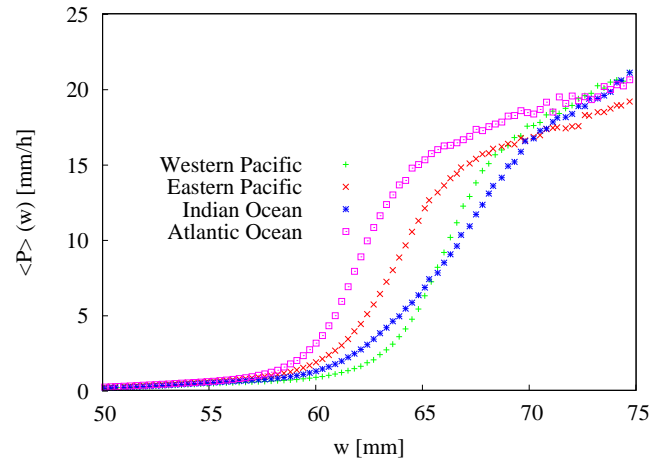


FIG. S1: **Order parameter, no rescaling:** As in Fig. 1 of main text for the order parameter $\langle P \rangle$, but showing all four regions without rescaling.

the order parameter $\langle P \rangle$ in Fig. S3, the collapses are good above the critical value w_c . Below w_c theory predicts an exact collapse only if the relevant system sizes (the size of the region that contributes to rainfall processes here), shapes and boundary conditions are equal. Eq. (1) of the main text applies only above w_c and is strictly only true for infinite systems. Finite systems tend to quickly approach this asymptotic behaviour above w_c . In our case, the curves for three of the regions collapse reasonably well near criticality, with the Indian Ocean showing a slightly less sharp increase in $\langle P \rangle(w)$ below w_c .

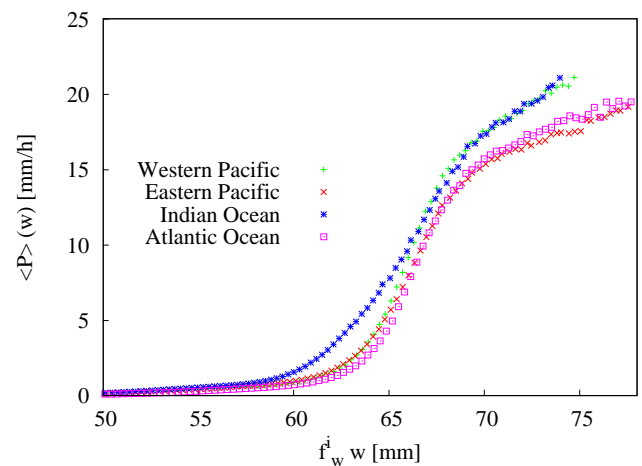


FIG. S2: **Order parameter, rescaled w :** Like Fig. S1, but including factors reflecting the different values of w_c .

The physical processes determining the rescaling factors for the different regions will be a tempting target

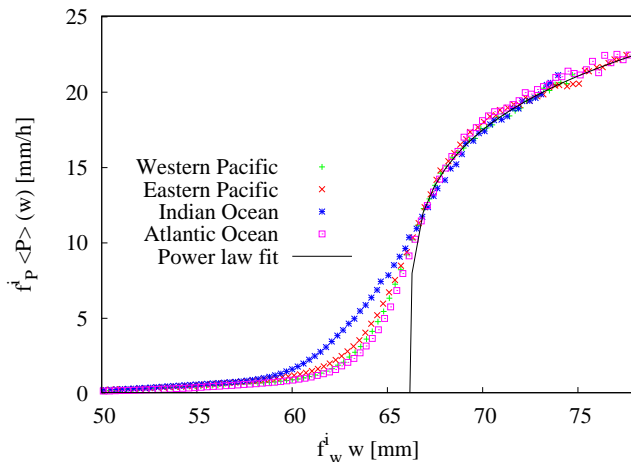


FIG. S3: **Order parameter, rescaled w and $\langle P \rangle(w)$:** Like Fig. S2 but including additional factors accounting for the different regional capacities to produce rainfall.

for subsequent work. Preliminary considerations suggest that this dependence will not be trivial. The values of w_c are smaller than those for saturation with respect to liquid water for typical temperatures and may be conjectured to also reflect buoyancy considerations. The factors f_P^i are not monotonic with w_c (for instance, the Eastern Pacific requires a larger factor than the Atlantic despite having higher w_c) and thus likely include factors more complex than just smaller column water content yielding smaller maximum rain rates. We speculate that considerations akin to tropical cyclone potential intensity theory [1, 2] involving differences between tropospheric temperature and SST may be relevant. However, development of such theory is beyond the scope of the present work.

B. Order parameter pick-up in liquid water

The TMI data set contains a cutoff in rain rate at 25 mm/h. Because this condition occurs more often at high water vapour levels, it is necessary to find measures to assess the impact on our results. In the microwave instrument retrieval algorithm, cloud liquid water and rain rate are not independent; there is an empirical partition between cloud water (drops with negligible fall speed) and rain water. Large values of cloud water are also a good measure of convection, so cloud liquid water could alternately have been used as an order parameter. We present precipitation in the main text because the loss of water from the atmosphere in the ensemble average acts to return the system to lower water vapour values (and because it is an important variable in human terms). In Fig. S4 we present the ensemble averaged cloud liquid water $\langle c \rangle(w)$ as a function of w , even though we expect similar results, because it provides a check on the impacts of the rain rate cutoff. The measurement-imposed cutoff on observations of cloud liquid water is 2.5 mm, and this

level is not reached at any time or location in the 5 years of data we investigated. Importantly, the sharp increase and subsequent saturation of this observable occurs at the same point as that for the rain rate. We conclude that the effects of the measurement-induced cutoff on the observed rain rate is insignificant. The power-law exponent for $\langle c \rangle(w)$ is about half that of the rain rate, $\beta_{\text{cloud}} \approx 0.13$ because for large rain rates c is approximately proportional to $P^{1/2}$ in the empirical relationship used in the retrieval algorithm.

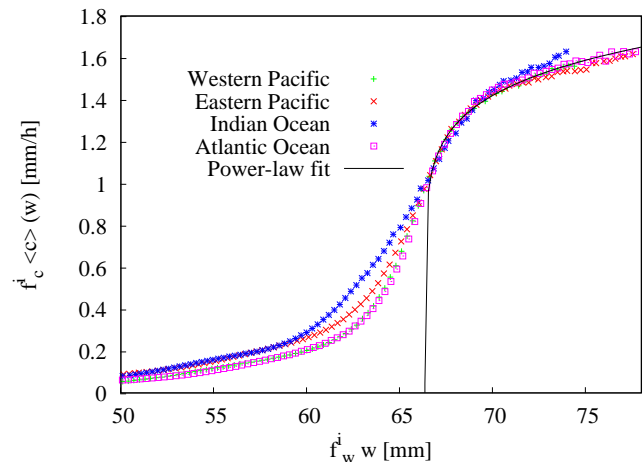


FIG. S4: **Cloud liquid water:** The solid line is a power-law fit. The curves for cloud liquid water have been rescaled with factors f_w^i in the w -axis, identical to those for the rainfall. The factors f_c^i are different from those for the rain rates, f_P^i . The critical water vapour derived from cloud liquid water is $w_c^{\text{cloud}} = 66.35$ mm, differing from the value for the rain rate by no more than 0.1 mm.

II. SUPPLEMENTARY DISCUSSION

A. Sea surface temperature dependence

In this section we quantify the statement that conditioning averages $\langle P \rangle(w)$ on sea surface temperature (SST) does not alter the results of our investigations significantly. In long-term climatological averages, regions of the highest tropical precipitation tend to correspond to higher SST, partly because it affects the large-scale slow driving of the system. At the time scales of the strong precipitation events considered here, this should be less of a factor than atmospheric temperature, which is not available in the data set we used. However, SST might provide a proxy for atmospheric temperature and moisture in the lower kilometre, or for differences in the large-scale forcing, and so it is of interest to examine the degree to which results change when stratified by SST. One might anticipate an increase of w_c with SST. To some extent this is true, as seen in the sequence of $\langle P \rangle(w)$ -curves conditioned on increasing SSTs in Fig. S5 for the

Atlantic Ocean. However, the main result is how remarkably similar the curves are over a considerable range of SST (for lower or higher SST values the ensemble of observations becomes small and statistics are poor). More quantification of this and of an expected dependence on tropospheric temperature is the subject of ongoing work.

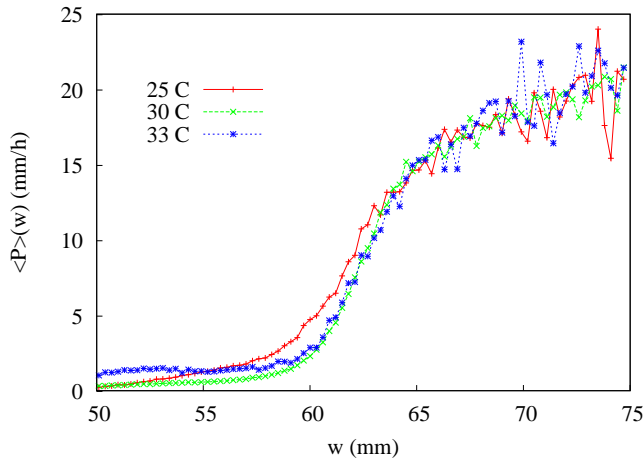


FIG. S5: **Different sea surface temperatures:** Ensemble mean precipitation as a function of column-integrated water vapour $\langle P \rangle$ from the Atlantic region; similar to Fig. 1 of the main text but conditioned on SST in 1 degree bins centred on 25, 30 and 33° C.

B. Synoptic examples

Raw maps of examples of the column-integrated water vapour w and precipitation observations on particular days are provided in Fig. S6 for orientation in terms of the typical meteorological situation. From a random sample of 6 days for the set of ascending satellite passes for each of the regions, maps were chosen on the following subjective criteria: eliminating examples with few high precipitation points since the information in such a map is low; a preference against cases where the satellite swath cuts off obvious interesting features; and a subjective sense of representativeness based on examination of a much wider sample. The averaging period in each 25 km pixel is very short (the resolution of the instrument scan); the satellite overpasses yielding separate swaths are roughly an hour and a half apart.

The region with w over 40-50 mm tends loosely to correspond to regions of warmer SST, although advected by variable large-scale circulation features. Within this region, local areas of higher w , within and above the critical w range seen in Fig. S1, have a higher occurrence of strong precipitation pixels. As expected from the high precipitation variance near w_c , this association is far from one to one, but tends to come out in averages conditioned on w over sufficiently large ensemble averages, at minimum several days.

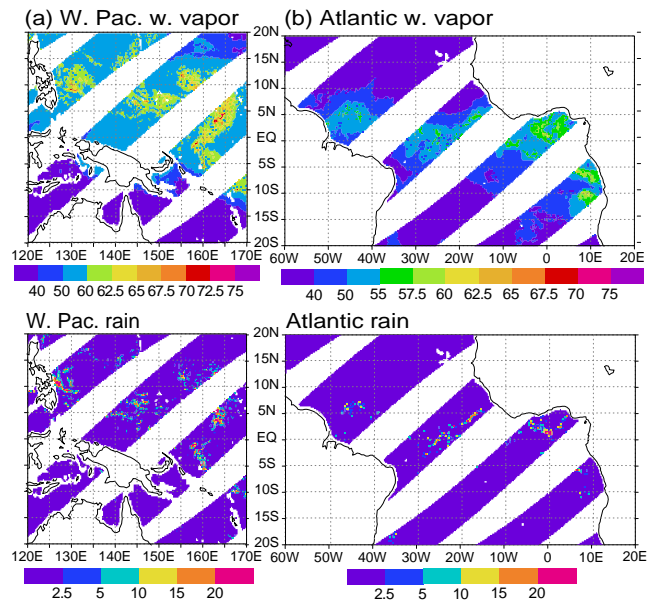


FIG. S6: **Synoptic examples:** TMI Column integrated water vapour (mm) and rain rate (mm/hr) for (a) the Western Pacific region on 10/08/2002. (b) the Atlantic region on 3/19/2001. White regions imply no data, typically between satellite swaths or over or near land points (including islands). The water vapour col or bar is chosen to provide higher resolution through the critical region and higher, and therefore differs between the regions. The precipitation col or bar is chosen to highlight the strong precipitation regime.

The Western Pacific case in Fig. S6a is an example of a relatively active region and day in terms of the number of intense precipitation points; the Atlantic case in Fig. S6b is an example of moderate activity. In both cases, a substantial fraction of the strong precipitation points occur within mesoscale precipitation features, as expected from much work in the meteorological literature [3–5]. A working definition of a mesoscale convective system is [6] “a cloud system that occurs in connection with an ensemble of thunderstorms and produces a contiguous precipitation area 100 km or more in horizontal scale in at least one direction.” For any of the intense precipitation features seen here, the association with strong deep convective elements is almost certainly met. While noting the caveat that some features contiguous in measurement with this instrument might not be if a high resolution radar was used, features with rain rates exceeding the first contour interval over a dimension equivalent to 1 degree latitude or more may be taken as examples of mesoscale systems. These include linear “squall line” features and loosely clumped aggregates. Such clusters, which are known to exhibit spatial scaling behaviour [7], must account for the power-law properties under spatial averaging of the precipitation variance up to scales of at least $(200 \text{ km})^2$ shown in the main text.

III. SUPPLEMENTARY EQUATIONS

A. Nontrivial variance-decrease implies scale-free correlation decay

In this section we show for a homogeneous and isotropic system comprising many degrees of freedom the relationship between the variance of averages taken over increasingly large areas in the system and the spatial decay of correlations. Remarks on how this homogeneous, isotropic case relates to the observed system—and why examination of the finite-size scaling of the variance is useful in evaluating this system—are given at the end of the section.

We consider a general system in 2 dimensions. The system consists of L^2 degrees of freedom of size 1. Each degree of freedom i at position \mathbf{r}_i contributes a (fluctuating) amount $p_i(t)$ to some macroscopic observable $P(t; L) = \frac{1}{L^2} \sum_{i=1}^{L^2} p_i(t)$, averaged over a linear scale L .

The correlation function between individual degrees of freedom is defined as

$$g(\mathbf{r}_i, \mathbf{r}_j) = \langle p_i p_j \rangle - \langle p_i \rangle \langle p_j \rangle, \quad (1)$$

where the brackets indicate time averages (the positions \mathbf{r}_i and \mathbf{r}_j are fixed). For a homogeneous, isotropic system, this quantity depends only on the distance $r = |\mathbf{r}_i - \mathbf{r}_j|$, that is,

$$g(\mathbf{r}_i, \mathbf{r}_j) = g(r). \quad (2)$$

$P(t; L)$ is strictly an instantaneous value of a spatial average over a block of L^2 degrees of freedom. Apart from these block-averages, we assume in our data analysis a weak form of ergodicity. Observations from different spatial blocks of size $L \times L$ (in a given climatic region and for a given interval in water vapour) are treated as equivalent to observations of the same block at different times.

The variance of these averages is defined as

$$\sigma_P^2(L) = \langle P^2(L) \rangle - \langle P(L) \rangle^2.$$

In this case, brackets indicate the “ergodic average”, adding data from all relevant blocks in space and time and dividing by the total number of observations. Writing the block averages explicitly and continuing to denote ergodic averages as $\langle \rangle$, we obtain

$$\begin{aligned} \sigma_P^2(L) &= \frac{1}{L^4} \left(\left\langle \left\langle \sum_{i=1}^{L^2} p_i \sum_{j=1}^{L^2} p_j \right\rangle \right\rangle - \left\langle \left\langle \sum_{i=1}^{L^2} p_i \right\rangle \right\rangle \left\langle \left\langle \sum_{j=1}^{L^2} p_j \right\rangle \right\rangle \right) \\ &= \frac{1}{L^4} \left(\sum_{i=1}^{L^2} \sum_{j=1}^{L^2} (\langle p_i p_j \rangle - \langle p_i \rangle \langle p_j \rangle) \right) \\ &= \frac{1}{L^4} \left(\sum_{i=1}^{L^2} \sum_{j=1}^{L^2} g(\mathbf{r}_i, \mathbf{r}_j) \right). \end{aligned} \quad (3)$$

Using homogeneity, this scales as

$$\frac{1}{L^2} \sum_{j=1}^{L^2} g(\mathbf{r}_i, \mathbf{r}_j). \quad (4)$$

The free index i indicates that the system is homogeneous—the integral will yield the same value, irrespective of the reference position \mathbf{r}_i . For an average with periodic boundary conditions, Eq. (3) is equal to Eq. (4). For a system with free boundary conditions where not all sites have the same number of neighbours at a given distance, this is modified by a constant factor and boundary effects whose contributions vanish as L increases. Assuming that the number of degrees of freedom is large also allows the sum to be approximated by an integral

$$\sigma_P^2(L) \approx \frac{1}{L^2} \int_A g(r_i, r_j) dr_j, \quad (5)$$

with A denoting the area of a block. Since only the scaling behaviour in L of the integral is of interest, effects of shape and boundaries of the system can be neglected. Thus we may switch the geometry to a convenient circle of equal area and solve the integral.

$$\sigma_P^2(L) = \frac{1}{L^2} \int_0^{L/\sqrt{\pi}} 2\pi r g(r) dr. \quad (6)$$

Given that $\sigma_P^2(L)$ is a power law $L^{-\lambda}$ with nontrivial $\lambda \neq 2$, we conclude that the integral must be a power law in L , and hence $g(r)$ itself must be a power law. Hence the observation of a non-trivial power-law decay of the variance $\sigma_P^2(w; L)$ in L near the critical point w_c implies a power-law decay of the correlation function under homogeneity and isotropy assumptions.

For the case of $g(r) = r^{-1.5}$, which corresponds roughly to our observations, we demonstrate in Fig. S7 the equivalence of the scaling behaviour numerically. While simple dimensional analysis ensures that the scaling behaviour of Eq. (6) is identical to that of the full double-sum in square geometry, Eq. (3), it is interesting to see the approach to the asymptotic behaviour for small systems.

Relationships between response functions like the susceptibility, fluctuations like the variance of the order parameter, and correlation functions are generally known as the fluctuation dissipation theorem, first described in Ref. [8]. A comprehensive review is provided in Ref. [9].

We now consider the applicability of the fluctuation dissipation theorem to the system observed here. The estimation of spatial correlation functions near criticality is challenging because even within a given climatic region, the column-integrated water vapour undergoes substantial variations in space and time. Here we sort the observations by w bin, so the proximity of the ensemble to criticality is known from other parts of the analysis. The ergodic ensemble consists of instances in time and space within a given climatic region of observations within a given w bin, averaged at scales of $L = 200$

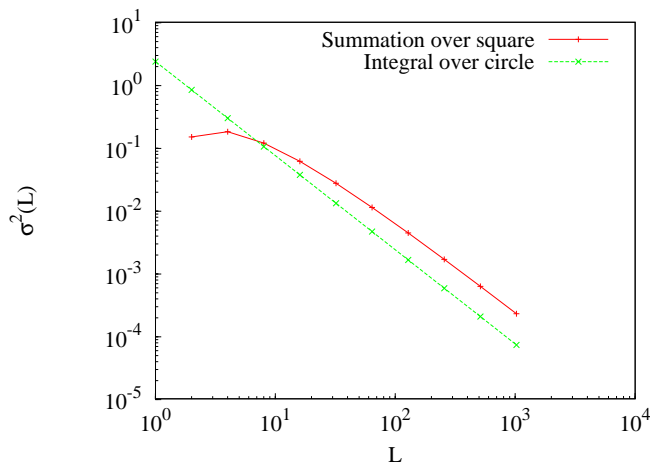


FIG. S7: **Integrated circle and summed square:** The green line shows the scaling of $\sigma^2(L)$ of the integrated circular geometry for $g(r) = r^{-1.5}$, Eq. (6), and the red line shows the corresponding summation in Eq. (3), evaluated in a square of equal area. For larger L the two lines continue as parallels, *i.e.* the asymptotic scaling behaviour has been reached.

km or less. The most important use of the homogeneity assumption in the derivation above is in simplifying sums over this spatial average. Under these conditions, homogeneity of the dominant physics affecting occurrence of strong precipitation appears justified. Isotropy is a very reasonable assumption for these scales and conditions. One potential source of anisotropy, the variation of the Coriolis force with latitude, becomes relevant on scales of thousands of km. Wind shear may break symmetry at particular times and locations but would have a broad distribution for the averages considered here.

Finally, we note that the caveats of the above derivation apply only to the claim that a scale-free decrease in precipitation variance implies a power-law form for the correlation function of rain rates at different locations. The observation that the precipitation variance conforms to expectations from critical systems is independent of this.

-
- [1] Emanuel, K. A. An air-sea interaction theory for tropical cyclones. Part I: Steady-state maintenance. *J. Atmos. Sci.*, **43**, 585–600 (1986).
 - [2] Bister, M., & Emanuel, K. A. Low frequency variability of tropical cyclone potential intensity I. Interannual to interdecadal variability. *J. Geophys. Res.*, **107**, 10.1029/2001JD000776 (2002).
 - [3] Houze, R. A., Jr., & Hobbs, P. V. Organization and structure of precipitating cloud systems. *Adv. Geophys.*, **24**, 225–315 (1982).
 - [4] Mapes, B. E., & Houze, R. A., Jr. Cloud Clusters and Superclusters over the Oceanic Warm Pool. *Mon. Wea. Rev.* **121**, 1398–1416 (1993).
 - [5] Nesbitt, S. W., Zipser, E. J., Cecil, D. J. A census of precipitation features in the tropics using TRMM: radar, ice scattering, and lightning observations. *J. Climate*, **38**, 4087–4106 (2000).
 - [6] Houze, R. A., Jr. *Cloud Dynamics*. (Academic Press Inc, San Diego, 1993).
 - [7] Perica, S., & Foufoula-Georgiou, E. Linkage of scaling and thermodynamic parameters of rainfall: results from mid-latitude mesoscale convective systems. *J. Geophys. Res.*, **101**, 7431–7448 (1996).
 - [8] Callen, H. B., & Welton, T. A. Irreversibility and generalized noise. *Phys. Rev.*, **83**, 34–40 (1951).
 - [9] Kadanoff, L. P., & Martin, P. C. Hydrodynamic equations and correlation functions. *Ann. Phys.*, **24**, 419–469 (1963).